Wiley Online Library
Early View publication on www.wileyonlinelibrary.com
(issue and page numbers not yet assigned;
citable using Digital Object Identifier – DOI)

J. Biophotonics 1–10 (2014) / **DOI** 10.1002/jbio.201300158

Journal of BIOPHOTONICS

FULL ARTICLE

Photonic crystal enhancement of a homogeneous fluorescent assay using submicron fluid channels fabricated by E-jet patterning

Yafang Tan[1], *Erick Sutanto*[2], *Andrew G. Alleyne*[2], *and Brian T. Cunningham*[*,1,3,4]

[1] University of Illinois at Urbana Champaign – Department of Electrical and Computer Engineering, 1406 West Green Street, Urbana, Illinois, USA
[2] University of Illinois at Urbana Champaign – Department of Mechanical Science and Engineering, 1206 West Green Street, Urbana, Illinois, USA
[3] University of Illinois at Urbana Champaign – Department of Bioengineering, 1304 West Springfield Avenue, Urbana, Illinois, USA
[4] 208 North Wright Street, Urbana, Illinois, 61801, USA

Received 7 October 2013, revised 18 November 2013, accepted 7 December 2013
Published online 24 December 2013

Key words: enhanced fluorescence, homogeneous assay, photonic crystal, submicron channel, E-jet printing

We demonstrate the enhancement of a liquid-based homogenous fluorescence assay using the resonant electric fields from a photonic crystal (PC) surface. Because evanescent fields are confined to the liquid volume nearest to the photonic crystal, we developed a simple approach for integrating a PC fabricated on a silicon substrate within a fluid channel with submicron height, using electrohydrodynamic jet (e-jet) printing of a light-curable epoxy adhesive to define the fluid channel pattern. The PC is excited by a custom-designed compact instrument that illuminates the PC with collimated light that precisely matches the resonant coupling condition when the PC is covered with aqueous media. Using a molecular beacon nucleic acid fluorescence resonant energy transfer (FRET) probe for a specific miRNA sequence, we demonstrate an 8× enhancement of the fluorescence emission signal, compared to performing the same assay without exciting resonance in the PC detecting a miRNA sequence at a concentration of 62 nM from a liquid volume of only ~20 nL. The approach may be utilized for any liquid-based fluorescence assay for applications in point-of-care diagnostics, environmental monitoring, or pathogen detection.

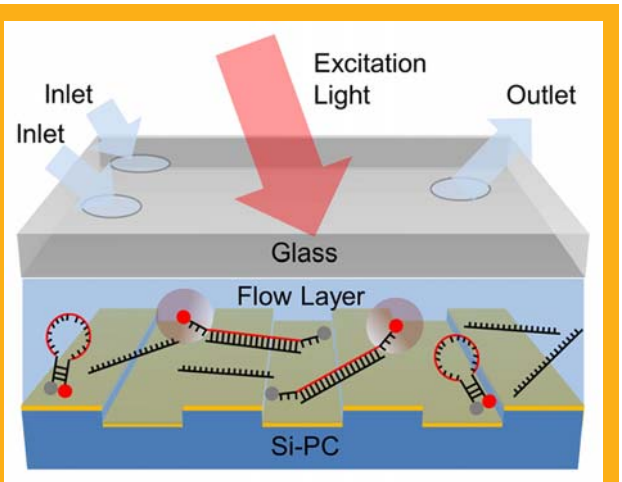

Schematic diagram of the sensor structure, comprised of a transparent glass layer, a microfluidic region and a PC surface for fluorescence enhancement

* Corresponding author: e-mail: bcunning@illinois.edu, Phone: 217–265-6291

1. Introduction

Due to the wide availability of dyes that can be easily conjugated to broad classes of biomolecules and detected with high sensitivity, fluorescence is the most widely used detection technique in life science research [1–4], disease diagnostics [5–7], and genomic/proteomic research tools [8–10]. Surface-based fluorescence assays, including DNA microarrays, protein microarrays, and fluorescence sandwich assays have achieved sensitivity gains of over two orders of magnitude by performing the assay protocol upon a nanostructured surface that is capable of enhancing the fluorescence excitation intensity of surface-bound fluorophores and by enhancing the collection efficiency of emitted photons [11–17]. A variety of nano-patterned structures including metal coated slides [18], plasmonic gratings [19, 20], 2D photonic crystals [21] and nanoantenna [22–24], have been studied for the purpose of enhancing the fluorescence output. In particular, photonic crystal enhanced fluorescence (PCEF) [11–13, 25], utilizes high quality factor resonances from a periodic dielectric surface structure to achieve high surface-bound electric fields that do not quench fluorescence emission.

While surface-based fluorescence assays are utilized for multiplexed assays in an array format, they are generally measured with a single endpoint scan, after all assay steps are completed and the assay surface is dry. However, many important classes of fluorescent assays are performed in a "homogeneous" format, with all assay components in a liquid environment, not coupled to a surface. For example, Fluorescence Resonant Energy Transfer (FRET) assays and Fluorescence Polarization (FP) assays are mainstays for disease diagnostics, pathogen detection, life science research, and toxin detection [26–30] that involve conjugation of fluorescent tags to at least one liquid-based assay component, in which the magnitude of the fluorescent output (for FRET) or the change in polarization of the fluorescent output (for FP) is determined by the concentration of a target analyte. Likewise, chemiluminescence assays and polymerase chain reaction (PCR) require detection of photon output from a LED or laser-illuminated liquid sample [31–33]. For each of these applications homogeneous assays require the ability to observe weak fluorescent signals above background autofluorescence for detection of biomolecular analytes at very low concentrations.

A fundamental limitation for the application of nanostructured surfaces for enhancing the fluorescence of homogeneous assays is that the enhanced electric field is tightly confined to the surface, with an evanescent field volume that extends only 100–600 nm into the liquid media in contact with the surface [34–38]. In order to achieve a substantial enhancement of the fluorescent output from a homogeneous assay using a nanostructured surface, it is necessary to confine the liquid volume so that a substantial proportion of it will reside within the evanescent field volume. Therefore, enhancement of the fluorescent output of homogeneous assays requires integration of the nanostructured surface and a fluid channel with a submicron height dimension.

A variety of approaches for creating microfluidic channels with submicron depth have been demonstrated through the application of photolithography [39, 40], sacrificial etching [41–44], and PDMS collapse [45–47]. However, these techniques either are low throughput, offer poor surface adhesion strength, or poor control of channel dimensions. The electrohydrodynamic jet (e-jet) printing approach used here is cost-effective, highly controllable and very simple. E-jet printing [48–50] is a nano-manufacturing process that uses electric field-induced fluid jet printing through micron-scale nozzles to achieve nanometer to micrometer-scale droplet placement accuracy and accurate control of ~0.5 pl dispense volumes. The printed fluid used in our approach is UV-curable optical adhesive (NOA74, Norland Products Inc., Cranbury, NJ). Assembly of the flow channel requires printing the adhesive pattern upon the PC substrate, attaching a glass cover with pre-drilled inlet/outlet holes to the PC surface, and curing by a short exposure to UV light. The approach can produce channels of arbitrary shape with micrometer-scale precision of lateral dimensions.

In this work, we demonstrate, to our knowledge, the first reported instance of fluorescence enhancement of a homogeneous assay using a nanostructured surface. We utilize a one-dimensional PC slab fabricated upon a silicon substrate as the enhancement surface that is designed to resonantly couple with a wavelength $\lambda = 637$ nm laser when the PC is covered in aqueous media. In order to achieve a submicron-height microfluidic channel that can be easily integrated with the PC, we demonstrate a new approach for creating a fluid channel, in which we print a pattern of droplets of light-curable adhesive using electrohydrodynamic jet (e-jet) printing. Rigorous Coupled Wave Analysis (RCWA) computer simulations were used to visualize the extent of resonant PC evanescent field into the volume of the flow channel, and to predict the electric field enhancement experienced by fluorophores extending through the channel volume. As an exemplary demonstration of homogeneous PCEF, we performed a FRET-based molecular beacon assay for detection of a specific miRNA sequence. Using a liquid volume of 20 nL to fill the nanochannel, we demonstrated up to 8× increase in fluorescence intensity by exciting the PC under resonant coupling conditions and detected the miRNA at a concentration as low as 62 nM.

2. Methods

2.1 Device structure and detection principle

The sensor structure is comprised of a transparent glass layer, the microfluidic channel region, and a PC surface for fluorescence enhancement (Figure 1a). As liquid flows through the channel, the fluorescent emitters will be excited by the laser illumination, with fluorophores closest to the PC surface experiencing electric fields that are amplified with respect to the incident laser intensity. Fluorescent emission is detected through the transparent glass cover.

The PC is comprised of a periodic surface structure fabricated in a low refractive index (RI) silicon dioxide (SiO_2) layer on a silicon substrate. The grating structure is coated with a high RI titanium dioxide (TiO_2) thin film. The PC has a period of 360 nm, a duty cycle of 36%, a grating depth of 40 nm, and a TiO_2 thickness of 130 nm. A commercial vendor (Novati Technologies Inc., Austin TX) was contracted for fabrication of PC surfaces over 8-inch diameter wafers, which were diced into 1.0×0.5 inch [2] pieces [14]. An SEM image showing the surface structure of the PC is presented in the inset of Figure 1b. Resonant modes of the PC can be excited at a specific incident angle for a given laser illumination wavelength [37]. At the resonance coupling condition of the PC, the enhanced electric fields are confined to the surface of the device, and extend into the adjacent media with exponentially decaying intensity as one moves away from the PC surface. By confining the assay solution to the evanescent field region of the PC, one can achieve an increase in the emission intensity of the dye throughout the channel. Our previous work demonstrated that the PC provides a wide Transverse Electric (TE) resonance at $\lambda \sim 685$ nm that provides an enhanced extraction effect. The extraction enhancement is ~1/4 of the excitation enhancement [51]. While the enhanced excitation effect can be turned off by illuminating the PC by an off-resonant wavelength/angle combination, the enhanced extraction effect is always present. The main benefit of enhanced extraction is increased collection efficiency of emitted photons by channeling them more efficiently in the direction of the instrument optical objective.

A commercially available simulation tool for RCWA (DIFFRACTMOD, RSoft) was used to characterize the device response to an incident transverse magnetic (TM) illumination source at $\lambda = 637$ nm. In the model, refractive indices were assigned using previously measured values for each material ($n_{TiO_2} = 2.35$, $n_{SiO_2} = 1.46$, $n_{Glass} = 1.52$, $n_{Water} = 1.33$) and device dimensions were used as specified in our previous description. The upper surface of the microfluidic channel was placed at a height of $t = 830$ nm, using values obtained from fabricated devices (Figure 2f).

We first calculated combinations of incident angle and wavelength that result in resonant coupling to the PC, at which electric field enhancement occurs [52]. Simulation predicts that, for a laser source of $\lambda = 637$ nm, the reflectance is maximized for an incident angle of $\theta = 1.55$ degrees with respect to normal. By Snell's Law, the corresponding resonant angle for illuminating the upper surface of the glass window, which should be used to compare with the experimental results, is $\theta_{air} = 2.39$ degrees. Simulation of the local electric field distribution at the reso-

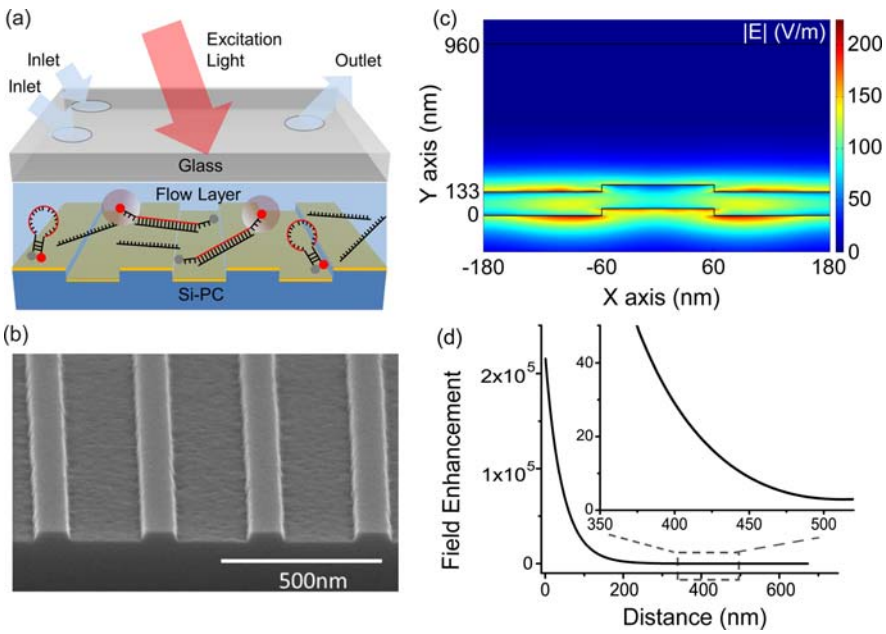

Figure 1 (**a**) Schematic diagram of the device structure, comprised of a transparent glass layer, a microfluidic region and a PC surface for fluorescence enhancement. (**b**) SEM image of the one dimensional PC with period of 360 nm and duty cycle of 36%. (**c**) Evanescent electric field enhancement distribution at the resonant coupling condition of the PC (**d**) The average enhancement of field intensity as the function of distance, d, above the top TiO_2 layer of the PC.

nant condition (Figure 1c), predicts that the maximum electric field enhancement is 225× the incident electric field magnitude of the laser, and shows that the greatest field enhancements occur within the TiO_2 film and in the regions in direct contact with the TiO_2. The simulations show that the field enhancement decays rapidly with increasing distance, d, from the PC, and that some regions on the PC surface experience greater electric field magnitude than others. To quantify the field enhancement as a function of d, taking into account the electric field distribution, we define the average enhancement factor F_{average} as the average intensity ($|E|^2$) enhancement of all the points in the simulation with a distance d from the PC surface. Mathematically, the averaged enhancement factor is defined as $F_{\text{average}}(d) = \int_0^{\Lambda} |E_{\text{local}}(x, d)|^2 \mathrm{d}x/\Lambda$, where $E_{\text{local}}(x, d)$ is the electric field enhancement at location (x, d). $F_{\text{average}}(d)$ is plotted with d ranging from 5 nm to 700 nm (Figure 1d), showing that the field enhancement decreases rapidly as one extends the liquid volume further from the PC surface. The zoom-in plot (inset of Figure 1d) suggests that no significant enhancement of the local intensity is observed when a fluorescent molecule is placed at a distance of ~500 nm from the PC surface, implying that the fluorescent molecules should be confined within the 500 nm volume above the PC in order to obtain a substantially enhanced fluorescence signal.

2.2 E-Jet printing of the submicron-channel

A novel fabrication method based upon e-jet printing was developed to create the submicron channels. Micron-size droplets of NOA74 were printed upon the PC substrate to form a channel pattern. Separately, a glass cover was prepared by drilling two inlets holes and one outlet hole. The glass cover and the epoxy-patterned PC were subsequently aligned and bonded by squeezing them together, followed by curing the adhesive by exposure to UV illumination.

The e-jet printing approach uses an electric field to induce droplet release flow from a micro capillary nozzle to the substrate, eliminating the need of a mask, while allowing precise printing of any desired pattern [49]. The microfluidic channel is 500 μm wide and 13.6 mm long, with a central detection region with a diameter of 2 mm. The assay region width was selected to fit the extent of the focused laser illumination line provided by the detection instrument. The channel lateral dimensions were defined by filling the regions surrounding the channel with printed droplets of adhesive, as shown in Figure 2a. In order to achieve a channel thickness as small as possible, NOA74 was chosen as the optical adhesive

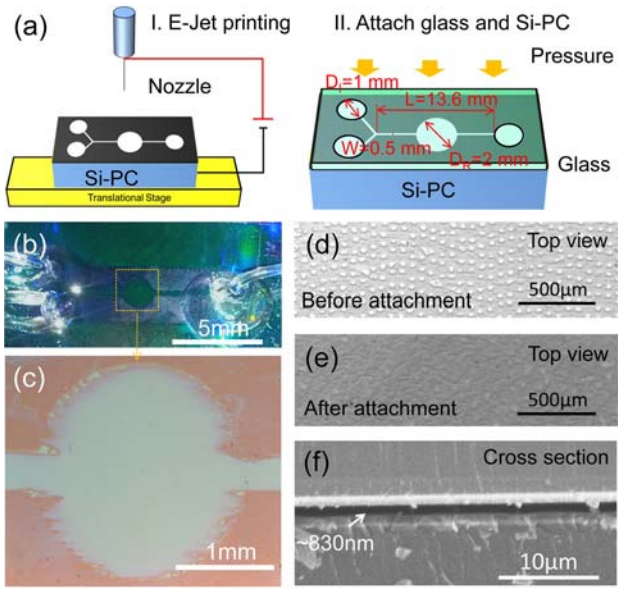

Figure 2 (**a**) Schematic diagram of the fabrication process: I. The channel pattern was e-jet printed on a silicon PC (Si-PC); II. The Si-PC was carefully aligned with a glass slide and pressed against each other by a roller to squeeze the droplets. The layout of the channel consisting of two inlets with diameters $D_I = 1$ mm (left), one observation window with a diameter $D_R = 2$ mm (middle), and one outlet with a diameter $D_I = 1$ mm (right). The total length and the width of the channel are $L = 13.6$ mm and $W = 0.5$ mm. (**b**) Photograph of the PC integrated into the submicron flow channel. (**c**) Optical image of the observation window. (**d**) Optical image of the printed NOA74 droplets. (**e**) Optical image of the continuous NOA74 film after squeezing the droplets. (**f**) SEM image of cross section of a completed device, showing the thickness of the channel is ~830 nm.

due to its low viscosity (80–95 cps) at room temperature. The droplet size and droplet density were selected to achieve a continuous adhesive film after the PC-glass attachment step, while avoiding the use of excessive material that would result in lateral flow, which would reduce the channel width. We used a gold/palladium (Au/Pd) coated nozzle with a tip diameter of 5 μm that was placed 30 μm from the continuously moving PC surface ($v = 1$ mm/s). The NOA74 was extracted [50] from the nozzle to the PC substrate to form discrete droplets, under a periodically modulated voltage (280 V high and 220 V low, 20 Hz) at room temperature and 30% humidity. The printing process required ~20 minutes to produce the pattern for one microfluidic channel. Each droplet occupies an area of ~20 × 30 μm [2], with 10–30 μm spacing between droplets (Figure 2d). The vertical height of the droplets before being squeezed was measured to be 1.2 ± 0.1 μm using a stylus contact profilometer (Alpha-Step IQ, KLA-Tencor Inc., CA), and the squeezing process is intended to re-

duce the adhesive height as the droplets spread to fill their surrounding volume.

To complete device fabrication, a glass cover was prepared with three holes (diameter = 1 mm) to match the inlets/outlet locations of the channel. The glass cover was then manually aligned with the printed PC substrate, which only required ~100 micron alignment accuracy to line up the inlet/outlet holes in the glass with the channel regions defined by the epoxy pattern on the PC. An evenly distributed force of ~100 N was applied at room temperature by a 20 lb Teflon-wrapped steel handheld roller. Uniformly applied pressure is an important key for achieving a uniform channel depth. We did not observe differences in fluorescence intensity within the 2 mm diameter measurement window. An optical image of the NOA74 after attachment to the glass cover is shown in Figure 2e, demonstrating that the droplets spread out and overlap with each other after squeezing. Finally, the adhesive was cured by exposing the assembly through the glass cover to a high intensity UV lamp (Xenon) for 50 seconds. Plastic tubing with inner diameter of 0.75 mm and outer diameter of 1 mm were inserted into the inlets and outlet and sealed with optical adhesive (NOA62, Norland Products Inc., CRANBURY, NJ) that was cured by a second exposure to the UV lamp.

A completed microfluidic assembly and a magnified view of the observation window are shown in Figure 2b, c. The two inlets are provided to enable separate introduction of the test sample and the assay label reagent, where they are allowed to mix within the central flow channel and assay region. For this work, measurements are performed while no flow occurs within the device. Between assays, buffer is introduced through both inlets, and waste is collected through the outlet port. Visual observation shows that smooth channel walls are obtained after droplet interdiffusion along the straight sections of the microfluidic channel, but that the channel edges are irregular surrounding the rounded detection region. Because the PC grating lines are oriented parallel to the microfluidic channel, we hypothesize that the compressed adhesive is able to preferentially flow along the low portions of the grating, and is less able to flow in the direction perpendicular to the grating. Cross section SEM images of the channel (Figure 2f) were used to measure a fluid channel height of 830 nm.

2.3 *Detection instrument*

A custom detection instrument was built to optimize coupling of laser illumination to the PC surface. As described in previously published reports, the excitation laser is collimated in the plane perpendicular to the grating lines, but focused in the plane parallel to the grating (Figure 4a). Collimated light with electric field polarization perpendicular to the grating lines is able to couple most efficiently with the PC resonant mode described in our computer model, but the light need only be collimated with respect to a single axis. Along the orthogonal axis, light can be focused without compromising coupling efficiency to the PC, and thus focus along one axis is used to achieve high illumination intensity. The system is designed for optimal interaction with the PC for both enhanced excitation and enhanced extraction, using design principles discussed, modeled, and demonstrated in Ref. [14]. The focal point of the cylindrical lens is located at the back focal plane of the objective, resulting a line of illumination in the PC that is collimated along the angle perpendicular to the PC grating lines, but focused in the orthogonal direction. Linear translation of the cylindrical lens results in adjustment of the incident angle to achieve 'on resonance' illumination. A semiconductor laser diode (AlGaAs, 70 mW, $\lambda = 637$ nm) is expanded to a diameter of 1 mm, and focused to an 8 μm wide line onto the PC surface by a cylindrical lens. A mirror coupled to a computer-controlled linear translation stage enables adjustment of the incident angle from 0–20 degrees with 0.01 degree increments. The grating lines of the PC are oriented perpendicular to the scan line, allowing the laser (polarized output perpendicular to the grating) designed to excite the TM mode of the PC.

3. Results

3.1 *Fluorescence enhancement characterization*

The resonant coupling condition of fabricated devices was experimentally determined by illuminating the PC through the glass cover while the channel is filled with water. The illumination was provided by a collimated white light source, while the reflected light was detected by a spectrometer (Ocean Optics Inc.). The device was mounted on a rotational holder, and the reflection spectra at different incident angles were recorded utilizing a commercial software package (Spectra suite, Ocean Optics Inc.). The spectrum with the resonant peak at $\lambda = 637$ nm indicates the condition where the laser can be efficiently coupled into the PC structure. The reflected spectra measured at the incident angle close to the surface normal (black solid line) and at ~2.4 degrees (resonance peak at the excitation wavelength of 637 nm, red dashed line) are presented in Figure 3,

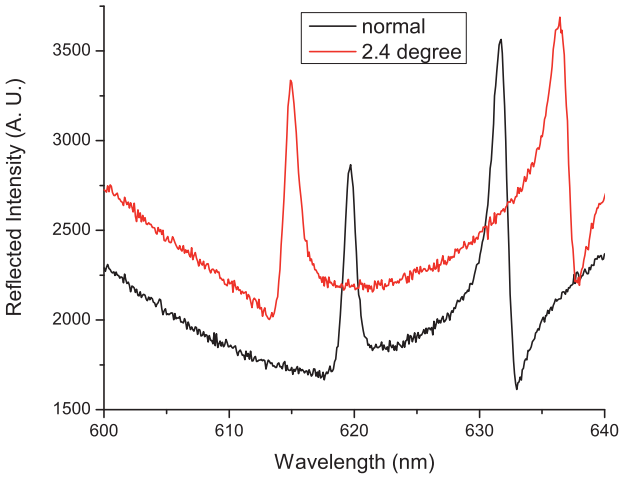

Figure 3 Reflection spectra of a device filled with water, illuminated with a broadband light source and captured at normal incidence (black, solid) and at an incidence angle of 2.4 degrees (red, dashed). At an incidence angle of 2.4 degrees, the resonant peak occurs at a wavelength of $\lambda = 637$ nm.

closely matching the coupling angle predicted by simulation.

The fluorescence intensity enhancement provided by the PC can be determined by comparing the fluorescent emission intensities from a channel with the PC surface illuminated at the resonant coupling condition (on-resonance) to measurement from the same channel when the PC is illuminated at an angle that does not satisfy the resonant coupling condition (off-resonance). The enhancement factor (EF) is defined as.

$$\mathrm{EF} = (I_{\mathrm{flou\_on}} - I_{\mathrm{bg\_on}})/(I_{\mathrm{flou\_off}} - I_{\mathrm{bg\_off}})$$

where $I_{\mathrm{flou\_on}}$, $I_{\mathrm{bg\_on}}$, $I_{\mathrm{flou\_off}}$ and $I_{\mathrm{bg\_off}}$ represent the fluorescence from a bulk dye solution and background fluorescence from buffer when the illumination of PC is on-resonance and off-resonance respectively. The *EF* was initially characterized by filling the fluid channel with a fluorescent dye (LD700, Exciton Inc., Dayton, OH, USA) dissolved in water at a concentration of 540 ng/mL, and measuring the fluorescent intensity $I_{\mathrm{flou\_on}}$, and $I_{\mathrm{flou\_off}}$ via illumination on-resonance ($\theta = 2.4$ degrees) or off-resonance ($\theta = 0.1$ degrees). The background fluorescence intensities $I_{\mathrm{bg\_on}}$ and $I_{\mathrm{bg\_off}}$ were determined by detecting the fluorescence from the device filled with DI water. The fluorescence intensity for each measurement is the sum of the fluorescence from the center of the illuminated area of 8 μm × 1mm. All of the fluorescence intensities were detected under the same instrument settings (laser current = 70 mA, and CCD gain = 1, sensitivity = 0, exposure time = 0.04 ms). The total amount of time to obtain a single angle spectrum is ~1 s and we did not observe reduction in fluorescent intensity over this time period due to photobleaching.

As shown in the angle spectrum (Figure 4b), the on-resonance fluorescence signal is $I_{\mathrm{flou\_on}} = 207\,584$ counts while the off-resonance fluorescence signal is $I_{\mathrm{flou\_off}} = 39\,472$ counts. The background fluorescence were measured as $I_{\mathrm{bg\_on}} = 57\,840$ counts and $I_{\mathrm{bg\_off}} = 21\,200$ counts for the respective off-resonance and on-resonance conditions. An enhancement factor of 8.2 can be calculated by applying the EF definition, representing the gain supplied by the enhanced excitation effect, indicating the potential to achieve an order of magnitude increase in fluorescence signal, compared to performing the same assay without a PC.

3.2 Bio-detection demonstration by molecular beacon assay

A homogeneous fluorescent assay using molecular beacon probes for detection of a specific miRNA sequence was performed by flowing solutions containing the molecular beacon probe and a sample containing the target miRNA simultaneously through the two inlets. Molecular beacon-based detection represents one class of FRET assay that has demonstrated strong potential for measurement of miRNA expression for applications including disease diagnostics and identification of novel therapeutic targets

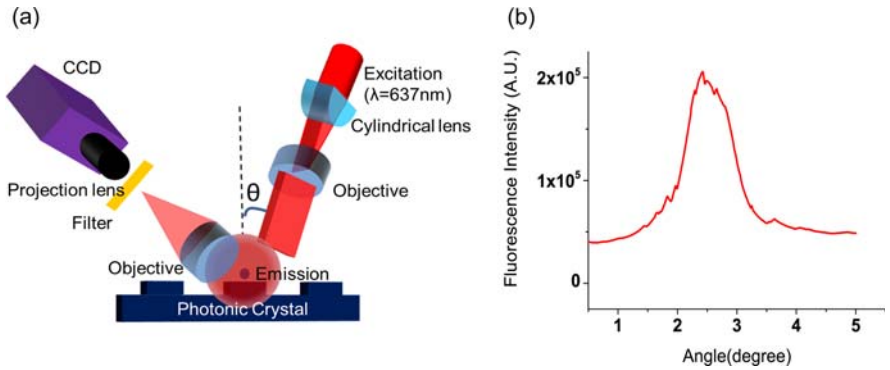

Figure 4 (**a**) Schematic diagram of the detection instrumentation. (**b**) Fluorescence intensities obtained from 0.5 μg/mL LD700 solution filled within the channel when excited over a range of illumination angles.

[53, 54]. Molecular beacons contain a stem-loop hairpin probe that is flanked by two short self-complementary sequences. A fluorescent dye and a suitable quencher for that dye are attached at each terminal of the short sequences so that their close proximity to each other will result in quenching of the fluorophore in the stem-loop structure. Adding target RNA that is complementary to the hairpin probe results in hybridization, which opens the hairpin probe that physically separates the quencher and the fluorophore, and allows the fluorophore to emit.

We utilized a previously reported molecular beacon probe and miRNA pair as an initial demonstration of PC enhanced fluorescence of a homogenous assay [55]. The molecule miR-21(5′-TAGCT TATCA GACTG ATGTT GA-3′) was the target while a mutant molecule miR-21 with a single base mismatch (5′-TA**A**CT TATCA GACTG ATGTT GA-3′, mismatched base is marked in bold) was used as a negative control for demonstration of selectivity. Both of the mutant miR-21 and the mature miR-21 were diluted by phosphate buffer sodium (PBS, pH = 7.4) into five concentrations ranging from 62 nM to 1 μM. The molecular beacon was designed to be complementary to the mature sequence of miR-21 (Cy5–5′-GCGCGT **CAACA TCAGT CTGAT AAGCT** ACGCGC-3′-BHQ2, the complementary region is indicated in bold). Each beacon consists of a 5′ Cy5 fluorophore, a 3′ BHQ2 quencher and a hairpin stem-loop sequence that is complementary to the mature miRNA flanked by residues necessary to form a beacon stem. The beacon solution was diluted to a concentration of 1 μM. The mature miR-21, mutant mature miR-21, and DNA molecular beacons were synthesized by Integrated DNA Technologies (Coralville, Iowa).

The performance of sensor and detection instrument were studied in the context of a molecular beacon assay for miR21. A 1 μM DNA molecule beacon solution and test sample containing mature miR21 were pumped into two separate inlets by a syringe pump (PHD2000 series, Harvard Apparatus) at a pumping rate of 0.5 μL/min for ~5 minutes. Waste liquid was collected at the outlet. The total volume inside the channel was calculated to be ~20 nL. After performing a fluorescence intensity measurement and flushing the system completely with deionized water, the detection experiment was repeated, using a new miR21 concentration. The concentrations of miR21 were 31 nM, 62 nM, 125 nM, 250 nM, 500 nM after dilution with the molecular beacon. After the channel was filled with test sample and molecular beacon solution, the solutions were allowed to stand in the channel for three minutes for complete mixing and hybridization by diffusion, as verified by performing the assay in a conventional 100 μL cuvette and measuring the output with a conventional fluorometer (Varian Cary Eclipse fluorometer, Agilent). Fluorescence intensities from the center of the observation window were collected over a range of incident angles for each concentration. The donor fluorophore of molecular beacon probe is not completely quenched when the probe is in its native unreacted state, resulting in the presence of "background" fluorescence, even if no target is present. A small fraction of molecular beacons that are open during thermal equilibrium may contribute to the observed background fluorescence. The background fluorescence is also amplified by PCEF, thus we expect to observe higher fluorescence intensity even for zero concentration of the analyte. We define the noise of the fluorescence measurement to be the standard deviation of the fluorescent intensity when no target molecule is present, in which the standard deviation is obtained by measuring the same zero concentration sample three times in a row. The lowest detectable fluorescence intensity is defined as the mean of these three measurements, plus 3× the standard deviation. The background fluorescence level was measured by this approach for the case when the PC is illuminated in the on-resonance state, and again with the PC illuminated at the off-resonant state. The off-resonance illumination is obtained by de-tuning the illumination angle by 2 degrees from the on-resonant angle. In order to demonstrate the selectivity of the assay, a concentration series of mutant mature miR21 (62 nM, 125 nM, 250 nM, 500 nM, 1 μM) were added into the 100 uL beacon solution as controls. The fluorescence intensities were obtained with the PC illuminated on-resonance and off-resonance for each concentration, and compared with that from the mature miR21. Detection instrument settings for measuring fluorescence output from the PC-integrated flow channel were the same for all measurements. (laser current = 80 mA, CCD camera sensitivity = 70, gain = 1 and integration time = 0.04 ms).

Dose-response curves for detection of mature miR21 (target, black lines) and mismatched mutant miR21 (control, blue lines), obtained from the device illuminated using on-resonance (solid lines) and off-resonance (dashed lines) conditions are plotted together in Figure 5(a). The comparison between fluorescence intensities at the same concentration both on-resonance and off-resonance clearly shows that much stronger fluorescence were produced by the PC surface. The enhancement was calculated to be ~8× for the miRNA mixture with concentrations higher than 62 nM. The Figure also demonstrated the selectivity of the assay. As shown in Figure 5(a), the fluorescence from the mutant mature miR21 with the highest concentration (500 nM) is only 1/7 of that from the mature miR21 at the on-resonance condition and no fluorescence was detectable in samples with concentration lower than 250 nM, demonstrating excellent selectivity.

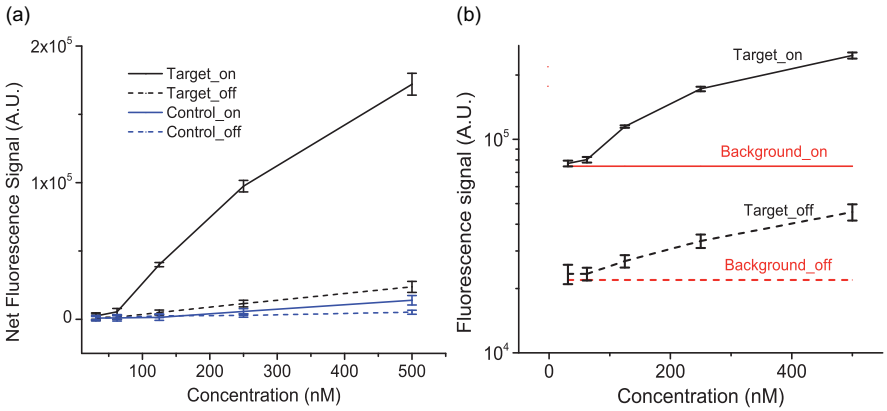

Figure 5 Results of the miR21 detection by DNA molecular beacon assay. (**a**) Dose response curves of mature miR21 (target, black lines) and one pair mismatched mutant miR21 (control, blue lines), obtained from PC at on-resonance (solid lines) and off-resonance (dashed lines) conditions. The results confirm the selectivity of the assay as well as the PCEF enhanced excitation effect. (**b**) A zoom-in plot of the fluorescence intensities for the detection of mature miR21 at on-resonance (black, solid line) and off-resonance (black, dashed line) conditions. The red lines represent the lowest detectable fluorescence at on-resonance (solid line) and off-resonance (dashed line) conditions.

To determine the detection limit, the fluorescent intensities of the hybridized target and the background are plotted together in Figure 5b. The solid black represents the on-resonance fluorescence intensities of the hybridized targets at different concentrations. The error bars represent the standard deviation of three separate fluorescence measurements for each concentration. The on-resonance lowest detectable fluorescence signal $Ml = 77\,200$ (the solid red line in Figure 5b), which was calculated by adding the background fluorescence $Mb = 74\,800$ and the noise $Sd = 800$, is slightly higher than the fluorescence from the 31 nM hybridized target. Therefore the detection limit for the on-resonance PC is 62 nM, representing a concentration that is within the range of interest for clinical applications [56]. The result demonstrates the high sensitivity of the biosensor, considering only ~0.02 μL sample solution was used to fill the channel, representing ~7.4×10 [6] molecular beacon probes for the assay. By comparing the fluorescence from the samples (dashed black line) and the lowest detectable fluorescence (dashed red line), the detection limit of the off-resonance PC is 125 nM. Although the background fluorescence was slightly enhanced, the sensitivity was still substantially improved utilizing the PC resonance effect.

4. Discussion and conclusion

We have demonstrated an 8× fluorescence intensity increase for detection of miRNA in a homogeneous molecular beacon assay by a PC as one of the internal surfaces of a microfluidic channel. The increased sensitivity enables detection of 62 nM miRNA in a 20 nL sample. Moreover, the optical signal amplification provided by the PC enables selection of a small and compact illumination source, such as the laser diode, and an inexpensive sensor to detect the output of assays that would otherwise be challenging. In order to confine the liquid volume within the evanescent field region of the PC, we developed an e-jet printing method to inexpensively fabricate fluid channels with <1 μm channel height that utilizes the PC as one internal surface.

The approached demonstrated here may be applied to any homogeneous fluorescent assay, including FRET, that is typically performed in a cuvette and measured by a conventional fluorometer, with the benefit of consuming a ~3-orders of magnitude lower sample volume. Another fluorescent assay that may potentially benefit from this approach is polymerase chain reaction (PCR), which requires several thermal cylces to create enough fluorescently-tagged products to generate a measurable signal from sample volumes in excess of 20 μL. The enhanced fluorescence provided by a PC integrated within a fluid channel may enable detection of PCR products with fewer cycles of amplification and thus a shorter detection time.

An important aspect of this work is that the fluorescence enhancement was achieved in a microfluidic format that permits the integration of functional components and allows high throughput detection. By multiplexing the operation of several parallel microfluidic chambers, the presence of multiple miRNA sequences may be probed at the same time.

To conclude, we have presented a novel method, supported by experimental demonstrations and nu-

merical modeling, to enhance the fluorescence of a homogeneous molecular beacon assay, in which the analyte solution is confined to the evanescent field region of a PC surface by a submicron-height microfluidic channel. A simple and inexpensive fabrication technique based on e-jet printing was developed to create the shallow channel. The approach yields excellent sensitivity while consuming only nL reagent volumes per assay. In light of the simplicity of the detection instrument and the compatibility with existing biodetection tools, this approach may be broadly applied in disease diagnostics and other fluorescence-based sensing applications.

Acknowledgement This work was supported by grants from the National Institutes of Health (GM086382A) and the National Science Foundation (CBET 07–54122). Any opinions, findings, conclusions, or recommendations expressed in this material are those of the authors and do not necessarily reflect the views of the National Institutes of Health or the National Science Foundation. The authors thank Yupeng Qiu (Department of Bioengineering) and Hang Xing (Department of Chemistry) for their helpful discussions on molecular beacon assay.

Author biographies Please see Supporting Information online.

References

[1] M. W. Elting, S. R. Leslie, L. S. Churchman, J. Korlach, C. M. J. McFaul, J. S. Leith, M. J. Levene, A. E. Cohen, and J. A. Spudich, Opt. Express **21**(1), 1189 (2013).
[2] J. S. Paige, T. Nguyen-Duc, W. Song, and S. R. Jaffrey, Science **335**(6073), 1194 (2012).
[3] A. F. Coskun, T.-W. Su, and A. Ozcan, Lab on a Chip **10**(7), 824 (2010).
[4] S. J. L. van Wijk, E. Fiskin, M. Putyrski, F. Pampaloni, J. Hou, P. Wild, T. Kensche, H. E Grecco, P. Bastiaens, and I. Dikic, Molecular Cell **47**(5), 797 (2012).
[5] L. S. Lim, M. Hu, M. C. Huang, W. C. Cheong, A. T. L. Gan, X. L. Looi, S. M. Leong, E. S.-C. Koay, and M.-H. Li, Lab on a Chip **12**(21), 4388 (2012).
[6] M. L. Y. Diakite, J. Champ, S. Descroix, L. Malaquin, F. Amblard, and J.-L. Viovy, Lab on a Chip **12**(22), 4738 (2012).
[7] S. Pang, C. Han, L. M. Lee, and C. Yang, Lab on a Chip **11**(21), 3698 (2011).
[8] K. A. Kolquist, R. A. Schultz, A. Furrow, T. C. Brown, J.-Y. Han, L. J. Campbell, M. Wall, M. L. Slovak, L. G. Shaffer, and B. C. Ballif, Cancer Genetics **204**(11), 603 (2011).
[9] W. Shi, C. A. de Graaf, S. A. Kinkel, A. H. Achtman, T. Baldwin, L. Schofield, H. S. Scott, D. J. Hilton, and G. K. Smyth, Nucleic Acids Research **38**(7), 2168 (2010).
[10] Q. Shi, L. Qin, W. Wei, F. Geng, R. Fan, Y. S. Shin, D. Guo, L. Hood, P. S. Mischel, and J. R. Heath, Proceedings of the National Academy of Sciences **109**(2), 419 (2012).
[11] P. C. Mathias, S. I. Jones, H.-Y. Wu, F. Yang, N. Ganesh, D. O. Gonzalez, G. Bollero, L. O. Vodkin, and B. T. Cunningham, Analytical Chemistry **82**(16), 6854 (2010).
[12] C.-S. Huang, S. George, M. Lu, V. Chaudhery, R. Tan, R. C. Zangar, and B. T. Cunningham, Analytical Chemistry **83**(4), 1425 (2011).
[13] C.-S. Huang, V. Chaudhery, A. Pokhriyal, S. George, J. Polans, M. Lu, R. Tan, R. C. Zangar, and B. T. Cunningham, Analytical Chemistry **84**(2), 1126 (2011).
[14] S. George, V. Chaudhery, M. Lu, M. Takagi, N. Amro, A. Pokhriyal, Y. Tan, P. Ferreira, and B. T. Cunningham, Lab on a Chip **13**(20), 4053 (2013).
[15] C. R. Sabanayagam and J. R. Lakowicz, Nucleic Acids Research **35**(2), e13 (2007).
[16] W. Hu, Y. Liu, H. Yang, X. Zhou, and C. M. Li, Biosensors and Bioelectronics **26**(8), 3683 (2011).
[17] S. M. Tabakman, L. Lau, J. T. Robinson, J. Price, S. P. Sherlock, H. Wang, B. Zhang, Z. Chen, S. Tangsombatvisit, J. A. Jarrell, P. J. Utz, and H. Dai, Nat Commun **2**, 466 (2011).
[18] J. Zhang and J. R. Lakowicz, Opt. Express **15**(5), 2598 (2007).
[19] X. Cui, K. Tawa, H. Hori, and J. Nishii, Advanced Functional Materials **20**(4), 546 (2010).
[20] P. Mandal, P. Gupta, A. Nandi, and S. A. Ramakrishna, Journal of Nanophotonics **6**(1), 063527 (2012).
[21] T. Kaji, T. Yamada, R. Ueda, and A. Otomo, The Journal of Physical Chemistry Letters **2**(14), 1651 (2011).
[22] C. Chiu, W. Xian, and C. F. Moss, presented at the Proceedings of the National Academy of Sciences of the United States of America, 2008 (unpublished).
[23] R. Zhang, Z. Wang, C. Song, J. Yang, and Y. Cui, J Fluoresc **23**(3), 551 (2013).
[24] Y. Fu, J. Zhang, and J. R. Lakowicz, Journal of the American Chemical Society **132**(16), 5540 (2010).
[25] S. George, V. Chaudhery, M. Lu, M. Takagi, N. Amro, A. Pokhriyal, Y. Tan, P. Ferreira, B. T. Cunningham, Sensitive Cancer Biomarker Detection Using Photonic Crystal Enhanced Fluorescence on a Silicon Substrate, submitted for publication (2013).
[26] H. Xu and M. Hepel, Analytical Chemistry **83**(3), 813 (2011).
[27] R. Häner, S. M Biner, S. M Langenegger, T. Meng, and V. L Malinovskii, Angewandte Chemie International Edition **49**(7), 1227 (2010).
[28] H. N. Joensson, C. Zhang, M. Uhlén, and H. Andersson-Svahn, Electrophoresis **33**(3), 436 (2012).
[29] T. Tachi, N. Kaji, M. Tokeshi, and Y. Baba, Lab on a Chip **9**(7), 966 (2009).
[30] Z.-L. Xu, Q. Wang, H.-T. Lei, S. A. Eremin, Y.-D. Shen, H. Wang, R. C. Beier, J.-Y. Yang, K. A. Maksimova, and Y.-M. Sun, Analytica Chimica Acta **708**(1–2), 123 (2011).

[31] C. Dodeigne, L. Thunus, and R. Lejeune, Talanta **51**(3), 415 (2000).
[32] S. Derveaux, J. Vandesompele, and J. Hellemans, Methods **50**(4), 227 (2010).
[33] Y. Zhang and P. Ozdemir, Analytica Chimica Acta **638**(2), 115 (2009).
[34] A. Pokhriyal, M. Lu, V. Chaudhery, C.-S. Huang, S. Schulz, and B. T. Cunningham, 2011 (unpublished).
[35] A. Pokhriyal, M. Lu, V. Chaudhery, S. George, and B. T. Cunningham, Applied Physics Letters **102**(22), 221114 (2013).
[36] S. George, V. Chaudhery, M. Lu, M. Takagi, N. Amro, A. Pokhriyal, Y. Tan, P. Ferreira, and B. T. Cunningham, Sensitive Cancer Biomarker Detection Using Photonic Crystal Enhanced Fluorescence on a Silicon Substrate, submitted for publication (2013).
[37] N. Ganesh, W. Zhang, P. C. Mathias, E. Chow, J. A. N. T. Soares, V. Malyarchuk, A. D. Smith, and B. T. Cunningham, Nat Nano **2**(8), 515 (2007).
[38] N. I. Cade, T. Ritman-Meer, K. A. Kwakwa, and D. Richards, Nanotechnology **20**(28), 285201 (2009).
[39] V. G. Kutchoukov, F. Laugere, W. van der Vlist, L. Pakula, Y. Garini, and A. Bossche, Sensors and Actuators A: Physical **114**(2–3), 521 (2004).
[40] A. Datta, S. Gangopadhyay, H. Temkin, Q. Pu, and S. Liu, Talanta **68**(3), 659 (2006).
[41] N. R. Tas, J. W. Berenschot, P. Mela, H. V. Jansen, M. Elwenspoek, and A. van den Berg, Nano Letters **2**(9), 1031 (2002).
[42] M. N. Hamblin, A. R. Hawkins, D. Murray, D. Maynes, M. L. Lee, A. T. Woolley, and H. D. Tolley, Biomicrofluidics **5**(2), 021103 (2011).
[43] Y. Song, M.-O. Kim, D.-S. Kwon, Y.-J. Kim, and J. Kim, Microelectronic Engineering **98**(0), 309 (2012).
[44] W. Sparreboom, J. C. T. Eijkel, J. Bomer, and A. van den Berg, Lab on a Chip **8**(3), 402 (2008).
[45] I. Choi, Y. S. Huh, and D. Erickson, Microfluid Nanofluid **12**(1–4), 663 (2012).
[46] S. H. Kim, Y. Cui, M. J. Lee, S.-W. Nam, D. Oh, S. H. Kang, Y. S. Kim, and S. Park, Lab on a Chip **11**(2), 348 (2011).
[47] K. L. Mills, D. Huh, S. Takayama, and M. D. Thouless, Lab on a Chip **10**(12), 1627 (2010).
[48] E. Sutanto, K Shigeta, Y. K. Kim, P. G. Graf, D. J. Hoelzle, K. L. Barton, A. G. Alleyne, P. M. Ferreira, and J. A. Rogers, Journal of Micromechanics and Microengineering **22**(4), 045008 (2012).
[49] J.-U. Park, M. Hardy, S. J. Kang, K. Barton, K. Adair, D. K. Mukhopadhyay, C. Y. Lee, M. S. Strano, A. G. Alleyne, J. G. Georgiadis, P. M. Ferreira, and J. A. Rogers, Nat Mater **6**(10), 782 (2007).
[50] S. Mishra, K. L. Barton, A. G. Alleyne, P. M. Ferreira, and J. A. Rogers, Journal of Micromechanics and Microengineering **20**(9), 095026 (2010).
[51] H.-Y. Wu, W. Zhang, P. C. Mathias, and B. T Cunningham, Nanotechnology **21**(12), 125203 (2010).
[52] N. Ganesh and B. T. Cunningham, Applied Physics Letters **88**(7), 071110 (2006).
[53] S.-X. Han, X. Jia, J.-l. Ma, and Q. Zhu, Arch. Immunol. Ther. Exp. **61**(2), 139 (2013).
[54] E. Chang, M.-Q. Zhu, and R. Drezek, Biotechnology Journal **2**(4), 422 (2007).
[55] M. B. Baker, G. Bao, and C. D. Searles, Nucleic Acids Research **40**(2), e13 (2012).
[56] M. Folini, P. Gandellini, N. Longoni, V. Profumo, M. Callari, M. Pennati, M. Colecchia, R. Supino, S. Veneroni, R. Salvioni, R. Valdagni, M. Daidone, and N. Zaffaroni, Molecular Cancer **9**(1), 12 (2010).

